Nanophotonics 1 (2012): 125–129 © 2012 Science Wise Publishing & De Gruyter • Berlin • Boston. DOI 10.1515/nanoph-2012-0004

Research Article

Measurement of the polarization state of light using an integrated plasmonic polarimeter

Farzaneh Afshinmanesh, Justin S. White, Wenshan Cai and Mark L. Brongersma*

Geballe Laboratory for Advanced Materials, Stanford University, 476 Lomita Mall, Stanford, CA 94305, USA, e-mail: brongersma@stanford.edu

*Corresponding author

Abstract

Plasmonics has started to facilitate the replacement of bulky optical components in optical systems by compact nanometallic elements that perform the same function. This allows for a natural and very dense integration with electronic devices. In this vein, we present a silicon (Si) photodetector integrated with a set of plasmonic structures that can be used as either a broadband linear-Stokes polarimeter or a narrowband full-Stokes polarimeter capable of determining the complete state of polarization of a light beam. At a probe-wavelength of 830 nm, our experimental results show contrast ratios of 25 and 1.13 for orthogonal linear and circular states of polarization, in good agreement with simulations. The resulting device is lightweight, orders of magnitude smaller than conventional polarimeters, and mechanically robust. For these reasons, there promises to be a wide range of applications including polarimetric imaging and sensing.

Keywords: Surface plasmon; polarization selective devices; polarimetry.

Polarization is a property of light that describes the vector nature of its electric field oscillations. Since polarization information is not correlated with the intensity or spectral information of light, use of polarized light has added superb capabilities to a wide range of applications including optical communications, imaging, microscopy, and sensing. In such applications, the state of polarization is typically monitored with the help of bulky optical components. It is by now well-established that nanometallic (i.e., plasmonic) structures can be engineered to produce an optical response that is strongly polarization-dependent [1–9]. Very recently, the use of plasmonic crystals in free-space polarimetric systems has even been demonstrated [10, 11]. Here, we show how to fully integrate plasmonic polarimetry functions with a Si-based photodetector. Such an integrated plasmonic polarimeter enables an accurate measurement of the complete state of polarization of light. Whereas conventional polarimetry approaches rely on the use of large optical components such as rotating polarizers and retardation wave plates, [12, 13] this work shows that a compact platform can achieve the same functions. This work adds to a growing body of literature where plasmonic elements can be integrated with semiconductor elements to produce photodetectors with enhanced optical responses, integration advantages, or new, built-in optical functionalities [14–17].

A set of four parameters is required to completely describe the state of polarization of an arbitrary polarized electromagnetic wave [12]. Experimentalists commonly use the Stokes parameters (S_0, S_1, S_2, S_3) for this purpose as these parameters are conveniently measured as a sum or difference of measurable light intensities after light passes through polarization sensitive filters [18]. We have designed a compact plasmonic photodetector structure with which these parameters can be quantified in a quick and convenient fashion through a set of photocurrent measurements.

Figure 1 schematically shows our envisioned plasmonic polarimeter, which consists of a silicon (Si)-based Schottky detector of which the gold (Au) contact is patterned with four linear subwavelength slits at different orientations and two subwavelength coaxial apertures surrounded by spiral grooves with opposite twists. A Schottky barrier is created by using a few nanometer thick chromium (Cr) layer between the n-type Si substrate and the Au layer. In this letter, we illustrate how the intensity measurements required determining the Stokes parameters can be translated into photocurrent measurements on the patterned structures. These photocurrent measurements then enable a convenient determination of the polarization state of an arbitrary polarized incident light beam.

Figure 1 shows a Cartesian coordinate system (x,y,z) with the light propagation direction along the z-direction and with electric field components E_x and E_y in the x and y directions. If we denote the light intensity of a beam that passes through a linear polarization filter oriented at an angle of θ° with respect to the x-axis by I_θ, then we find that $S_0=I_0+I_{90}$ is the intensity of the original light beam. The other Stokes parameters are given by $S_1=I_0-I_{90}$ and $S_2=I_{45}-I_{135}$ and represent the difference between light intensities after passing through two different sets of orthogonally polarized filters. The last Stokes parameter is given by $S_3=I_{RHC}-I_{LHC}$ and quantifies the difference between intensities of the right-handed and left-handed circularly polarized portions of the light [12]. Based on these definitions, all four Stokes parameters can thus be determined through six intensity measurements behind four filters for linear polarization and two filters for circular polarization [19]. In the following sections, we will show how the six required polarization filters can be implemented with differently shaped plasmonic structures patterned in the Au film. Given the linear relationship between the generated photocurrent and the light intensity behind the filters in the Si substrate, the

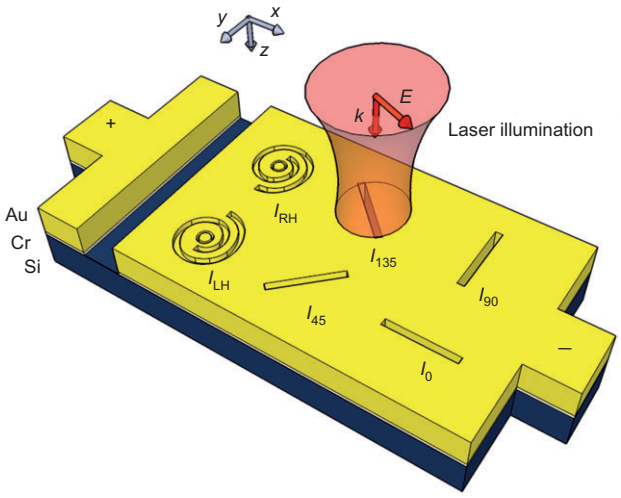

Figure 1 Schematic diagram of the proposed plasmonic polarimeter that consists of six, differently shaped plasmonic slit structures patterned into an Au film on top of a Si-based Schottky detector. Photocurrent measurements on different plasmonic structures enable a direct determination of the state of polarization of an incident light beam.

required intensity measurements can effectively be translated into a set of photocurrent measurements.

It has been shown that linear slits in a metal film give rise to extraordinary optical absorption when placed on an absorbing material [20]. In a detector structure as shown in Figure 1, this absorption can be directly quantified in a photocurrent measurement. For a linear slit, light absorption is maximized when the electric field of the incident light is polarized normal to the slit and is dramatically reduced when the electric field is parallel to the slit. For this reason, the measured photocurrent obtained from an illuminated linear slit is essentially related to the portion of the light polarized normal to the slit. We have arranged four linear slits in an Au film on a Si substrate as filters for linear polarization shown in Figure 1 and 3A. We have numerically and experimentally investigated the polarization-dependent transmission properties of these slits.

We have modeled the transmission of light through a linear slit in an Au film on a Si substrate using a finite element method employing COMSOL Multiphysics. Figure 2A depicts this device along with the corresponding magnetic field distribution for a transverse magnetic (TM) polarization with the electric field normal to the slit. A monochromatic plane wave with an 830 nm wavelength traveling in *z*-direction impinges upon a 100-nm wide slit in a 200-nm thick Au film. The material parameters are obtained from Ref. [21]. The simulations are performed in two dimensions (*yz* plane) and in COMSOL Hybrid Mode, which allows a rotation of the electric field in the *xy* plane and analyzing the polarization-dependant absorption of light in the Si beneath the slit. The angle of the incident electric field rotates from 0 (electric field along the slit) to 360° and the corresponding absorption in the Si is calculated. Figure 2B shows the calculated normalized absorption as a function of the polarization angle. The linear polarization contrast ratio (LPCR), which is defined

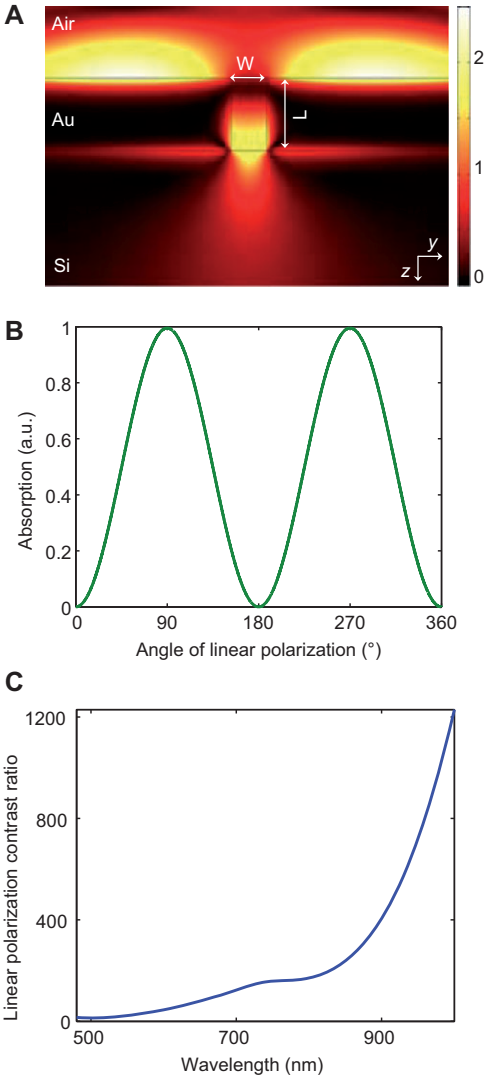

Figure 2 (A) Magnetic field distribution ($|H_x|$) for the slit detector on a Si substrate. The thickness of Au (L) is 200 nm and the gap size (W) is 100 nm. The slit is illuminated from the top with a plane wave whose electric field is polarized in *y*-direction (TM polarization). (B) Absorption in the Si is calculated as a function of the angle between the incident electric field and the slit at 830 nm wavelength. The absorption is normalized to the absorption calculated for TM polarization. (C) The calculated linear polarization contrast ratio as a function of the illumination wavelength.

as the ratio between the maximum and minimum absorption, is calculated to be 200 at 830 nm. The LPCR at a certain wavelength and for a certain choice of metal depends on geometrical parameters and it can be maximized by tuning these parameters, i.e., increasing the metal thickness. If we keep the Au thickness and slit gap size constant and scan the wavelength, the LPCR monotonically increases as a function of wavelength as shown in Figure 2C. Increasing the slit width at a given wavelength would lower the LPCR signal. In some applications such as full linear Stokes imaging polarimetry [22], measurement of S_0, S_1, and S_2 is sufficient and measurement of all four Stokes parameters is not required since very

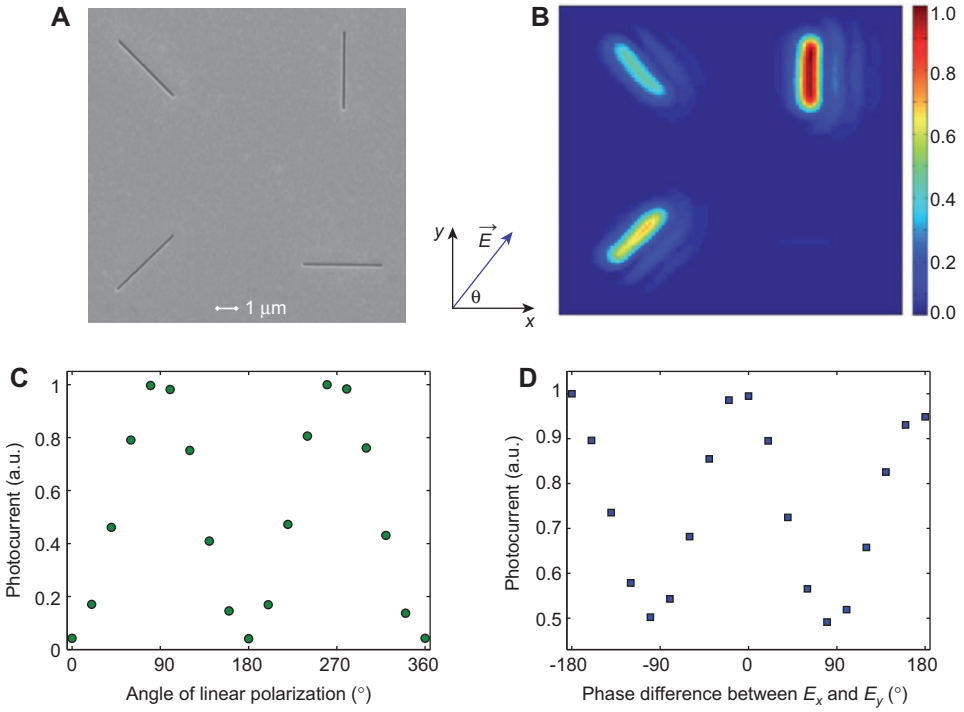

Figure 3 (A) Scanning electron microscopy (SEM) image of that part of the Stokes detector in which four linear slits are cut into the Au film with a focused ion beam. The slit widths are 100 nm and the slit lengths are 4 µm. This aspect ratio is sufficiently large to avoid edge effects. The separation between slits is 10 µm. (B) Measured photocurrent map of the linear Stokes detector for a linearly polarized incident beam. The angle between the incident electric field and the horizontal slit is 7° and the illumination wavelength is 830 nm. The photocurrent is normalized to the maximum measured photocurrent. (C) Normalized measured photocurrent of the horizontal slit as a function of the polarization angle of the incident linearly polarized light. (D) Normalized measured photocurrent of the horizontal slit as a function of the phase difference between E_x and E_y.

little amount of circular polarization is present. In these cases, the aforementioned arrangement of four slits would provide the complete polarization state over a wide wavelength range from visible to near IR.

The linear Stokes polarimeter is made in a 200-nm thick Au film with focused ion beam milling (FIB) as shown in Figure 3A. A 5-nm thick Cr layer is sandwiched between the Au film and the n-type Si substrate as an adhesion layer for the Au and to form a Schottky barrier. The Schottky barrier enables effective charge separation of the photogenerated carriers near the Si surface, right where the plasmon-enhanced optical fields are largest. In experiments, the light from an 830 nm diode laser is spatially filtered using a single mode optical fiber. It is then collimated and then passed through a polarizer, a half-wave plate, and finally focused to a ~1.5 µm diameter spot on the device with a microscope objective (50× objective with 0.42 NA). Modulation of the optical signal was used for lock-in based measurements. The device is mounted on a precision piezo-stage and electrically contacted using a set of wire-bonded contacts. The photocurrent images of the linear Stokes polarimeter are obtained by raster scanning the laser beam over the device. Figure 3B shows a photocurrent image obtained from the slit array for the case where the angle between the incident light electric field and the horizontal slit is 7°. This photocurrent image confirms that the light absorption in the Si is dominated by the portion of the light polarized normal to each slit.

The photocurrent response of a single slit at a given polarization is defined as the maximum measured photocurrent found in scanning the beam over the slit. Figure 3C shows the photocurrent response of a single slit as the direction of the incident electric field is continuously varied with a half wave plate. This behavior is consistent with the results in Figure 2B and we find a LPCR of 25 at the 830 nm wavelength.

To measure the response of a slit to elliptical and circular polarizations, we replace the half wave plate with a quarter wave plate. Figure 3D shows the photocurrent response of a single slit when we change the relative phase between x and y components of the electric field by a quarter wave plate. As expected, the measured photocurrent for linear polarization is twice of that for circular polarization.

So far we have introduced a broadband linear Stokes polarimeter with which we can distinguish between linear, circular, and elliptical states of polarization for polarized light and determine the degree of linear polarization ($\sqrt{S_1^2+S_2^2}/S_0$) for partially polarized light. To determine the handedness of a circularly or elliptically polarized light and also degree of circular polarization (S_3/S_0) for partially polarized light, we require filters for right-hand and left-hand circular polarizations.

It has been shown that spiral grooves or spiral slits respond differently to circularly polarized (CP) light of opposite handedness due to geometric phase effects [23–26]. Two Archimedean spiral grooves with opposite twists in an Au film are used to determine the direction of polarization rotation, as schematically shown in Figure 1. When a light beam impinges on the spiral groove, it excites surface plasmon polaritons (SPPs) on the Au surface. The interference pattern of the SPPs depends on the polarization of the incident light and the spiral twist. For CP light, the SPP interference pattern is an evanescent Bessel beam of order n where n depends on the number and direction of rotation of spiral grooves and the handedness of the CP light [26]. For a right-handed (RH) spiral groove, SPPs interfere constructively at the center of the groove for left hand circular polarization (a zero-order Bessel beam) and destructively for right hand circular polarization (a second-order Bessel beam). Figure 4 depicts simulation results of the electric field distribution at 1 nm above the Au-air interface for right and left hand circular polarizations (RHCP, LHCP) and two orthogonal linear polarizations illuminating an RH spiral groove.

By placing a coaxial aperture [27] with an appropriate size at the center of a spiral groove, different SPP interfence patterns for different polarizations can be translated into different amounts of light absorption in the Si detector. The advantage of using a coaxial aperture is that both the coupling of SPPs generated by a spiral to the coaxial aperture mode and the transmission through the coaxial aperture can be highly efficient. In contrast, poor transmission would be observed for a deep subwavelength coaxial aperture surrounded by a circular grating. By appropriately choosing the inner and outer radii of a coaxial aperture, we can maximize Si absorption when the spiral twist and handedness of the incident circular polarization are opposite and minimize absorption when they are the same.

At an 830 nm wavelength, we find from full-field 3D COMSOL simulations that good results can be obtained when the inner and outer radii of the coaxial aperture are 310 nm and 410 nm, respectively. In simulations, we illuminate a two-turn RH spiral groove with a Gaussian beam with 2.7 µm full-width half-maximum (FWHM) and measure the absorption in the Si substrate. The depth of the spiral groove is chosen to be 70 nm, the width is half a SPP wavelength, and the center-to-center distance between grooves is 813 nm, close

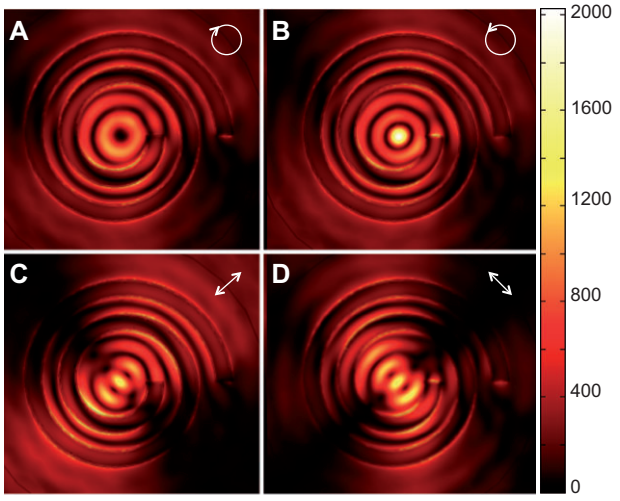

Figure 4 Simulation of the electric field distribution at the surface of an Au film patterned with an RH spiral groove and air. The spiral groove is illuminated with (A) RHCP, (B) LHCP, and (C, D) two orthogonal linearly polarized Gaussian beams at 830 nm. The direction of propagation of the beam is normal to the patterned metal surface.

to the SPP wavelength for a freespace wavelength of 830 nm. The circular polarization contrast ratio (CPCR), which is defined as the ratio between LHCP absorption and RHCP absorption, is calculated to be 1.96. For an LH spiral groove, the CPCR is inverse of that as expected. Using two-fold spiral grooves or adding more winding turns to the spiral grooves can increase the CPCR. The propagation length of surface plasmons ultimately limits the maximum achievable CPCR.

Figure 5A shows a scanning electron microscopy (SEM) image of a coaxial aperture surrounded by an RH spiral groove designed for an 830 nm wavelength. Figure 5B shows the measured photocurrent for the device shown in Figure 5A as a function of the phase difference between E_x and E_y. The measured CPCR with an illuminating beam spot of ~4 µm is 1.13. This experimental result together with the simulations show that we can determine the direction of polarization rotation by measuring the photocurrents from two apertures surrounded by spiral grooves with opposite twists. The sense of polarization can simply be determined by determining which

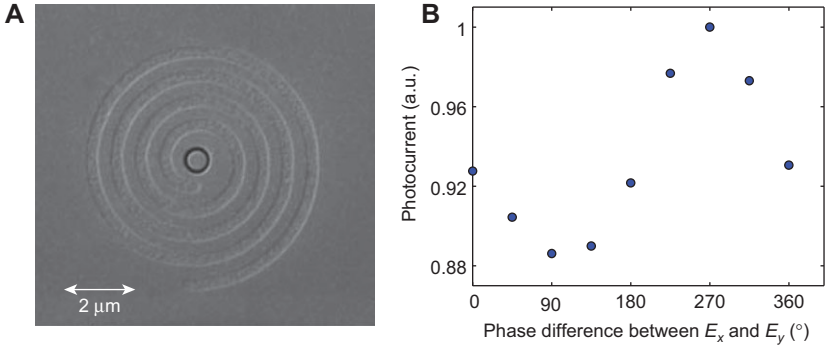

Figure 5 (A) SEM image of a coaxial aperture surrounded by an RH spiral groove fabricated with FIB. (B) Normalized measured photocurrent of the coaxial aperture shown in (A) as a function of the phase difference between E_x and E_y.

spiral produces the larger photocurrent. By introducing appropriate gain factors, we can match the gain of coaxial apertures to linear slits and extract full Stokes parameters from six photocurrent measurements.

In summary, we have introduced a plasmonic polarimeter integrated with a Si photodetector that can determine the complete polarization state of a beam of light. Measurement of the state of polarization typically requires bulky optical components. This work may impact the design of future, ultra-compact integrated systems and cameras that can monitor a variety of properties of light in a simple and efficient manner. In such designs, multiple, closely-spaced (<<1 μm), individually-addressable detectors or pixels can each be furnished with distinct plasmonic functionalities (e.g., polarization or color filtering) and the need for scanning (as in Figure 3) would be obviated.

Acknowledgments

The authors acknowledge the financial support from the Department of Energy, grant DE-FG02-07ER46426 and the Intel Corporation. The authors also gratefully acknowledge helpful discussions with R. Pala, A. Marandi, E. S. Barnard, Y. C. Jun, K. C. Balram and D. Ly-Gagnon.

References

[1] Genet C, Ebbesen TW. Light in tiny holes. Nature 2007; 445(7123):39–46.
[2] Fedotov VA, Schwanecke AS, Zheludev NI, Khardikov VV, Prosvirnin SL. Asymmetric transmission of light and enantiomerically sensitive plasmon resonance in planar chiral nanostructures. Nano Lett 2007;7(7):1996–9.
[3] Ziegler JI, Haglund Jr. RF. Plasmonic response of nanoscale spirals. Nano Lett 2010;10(8):3013–8.
[4] Gorodetski Y, Niv A, Kleiner V, Hasman E. Observation of the spin-based plasmonic effect in nanoscale structures. Phys Rev Lett 2008;101(4):043903.
[5] Drezet A, Genet C, Ebbesen TW. Miniature plasmonic wave plates. Phys Rev Lett 2008;101(4):043902.
[6] Schuller JA, Barnard ES, Cai W, Jun YC, White JS, Brongersma ML. Plasmonics for extreme light concentration and manipulation. Nature Materials 2010;9(3):193–204.
[7] Yu N, Fan J, Wang QJ, Pflugl C, Diehl L, Edamura T, Yamanishi M, Kan H, Capasso F. Small-divergence semiconductor lasers by plasmonic collimation. Nature Photon 2008;2(9):564–70.
[8] Jun YC, Huang KCY, Brongersma ML. Plasmonic beaming and active control over fluorescent emission. Nature Commun 2011;2:283.
[9] Kim H, Park J, Cho S, Lee S, Kang M, Lee B. Synthesis and dynamic switching of surface plasmon vortices with plasmonic vortex lens. Nano Lett 2010;10(2):529–36.
[10] Benetou MI, Thomsen BC, Bayvel P, Dickson W, Zayats AV. Four-level polarization discriminator based on a surface plasmon polaritonic crystal. Appl Phys Lett 2011;98(11):111109.
[11] Benetou MI, Thomsen BC, Bayvel P, Dickson W, Zayats AV. SPP5 Proceedings. 2011.
[12] Berry HG, Gabrielse G, Livingston AE. Measurement of the stokes parameters of light. Appl Opt 1977;16(12): 3200–5.
[13] Azzam RMA, Bashara NM. Ellipsometry and polarized light. Amsterdam: Elsevier, 1997.
[14] Ishi T, Fujikata T, Makita K, Baba T, Ohashi K. Si Nano-Photodiode with a surface plasmon antenna. Jpn J Appl Phys 2005;44:L364–6.
[15] Tang L, Kocabas SE, Latif S, Okyay AK, Ly-Gagnon D, Saraswat KC, Miller DAB. Nanometre-scale germanium photodetector enhanced by a near-infrared dipole antenna. Nature Photon 2008;2(4):226–9.
[16] Neutens P, Van Dorpe P, De Vlaminck I, Lagae L, Borghs G. Electrical detection of confined gap plasmons in metal-insulator-metal waveguides. Nature Photon 2009;3(5):283–6.
[17] Guillaumee M, Dunbar LA, Santschi CH, Grenet E, Eckert R, Martin OJF, Stanley RP. Polarization sensitive silicon photodiodes using nanostructured metallic grids. Appl Phys Lett 2009;94(19):193503.
[18] Stokes GG. On the composition and resolution of streams of polarized light from different sources. Trans Cambridge Philos Soc 1852;9:399.
[19] Stutzman WL. Polarization in electromagnetic systems. Boston: Artech House, 1993.
[20] White JS, Veronis G, Yu Z, Barnard ES, Chandran A, Fan S, Brongersma ML. Extraordinary optical absorption through subwavelength slits. Opt Lett 2009;34(5):686–8.
[21] Rakic AD, Djurišic AB, Elazar JM, Majewski ML. Optical properties of metallic films for vertical-cavity optoelectronic devices. Appl Opt 1998;37(22):5271–83.
[22] Walraven R. Polarization imagery. Opt Eng 1981;20:14.
[23] Gorodetski Y, Shitrit N, Bretner I, Kleiner V, Hasman E. Observation of optical spin symmetry breaking in nanoapertures. Nano Lett 2009;9(8):3016–9.
[24] Yang S, Chen W, Nelson RL, Zhan Q. Miniature circular polarization analyzer with spiral plasmonic lens. Opt Lett 2009;34(20):3047–9.
[25] Chen W, Abeysinghe DC, Nelson RL, Zhan Q. Experimental confirmation of miniature spiral plasmonic lens as a circular polarization analyzer. Nano Lett 2010;10(6):2075–9.
[26] Ohno T, Miyanishi S. Study of surface plasmon chirality induced by Archimedes' spiral grooves. Opt Express 2006;14(13):6285–90.
[27] Catrysse PB, Fan S. Understanding the dispersion of coaxial plasmonic structures through a connection with the planar metal-insulator-metal geometry. Appl Phys Lett 2009;94(23): 231111.

Received November 9, 2011; accepted February 14, 2012